Experimental study of Tilt-Wing eVTOL Take-Off Aerodynamics

H.N.J. Dekker[1], M. Tuinstra[2], W.J. Baars[1], F. Scarano[1] and D. Ragni[1]

[1]Faculty of Aerospace Engineering, Delft University of Technology
[2]Department of Vertical Flight and Aeroacoustics, Netherlands Aerospace Centre
hasse.dekker@nlr.nl

Abstract

The unsteady aerodynamic interactions during the vertical take-off of an Over-The-Wing mounted rotor array are experimentally investigated. The wing's geometric angle of attack and wind tunnel velocity change dynamically during acquisition, corresponding to a reference tilt-wing flight trajectory. Simultaneously, the flow is characterized using large-scale Lagrangian Particle Tracking employing helium-filled soap bubbles as tracer particles. The measurements return the three-dimensional aerodynamic interactions that occur during the flight maneuver. The results are compared with measurements that have been obtained in a quasi-steady way. This comparison shows only minor differences and therefore does not indicate the presence of any transient effect, although a more detailed analysis is required to conclude this.

1 Introduction

Advancements in battery technology have resulted in the rise of electric Vertical Take-Off and Landing vehicles (eVTOLs)[7]. These vehicles use disruptive designs for the propulsion system, resulting in unexplored aerodynamic interactions between the propulsors and lifting surfaces [1]. The tilt-wing [3] is an example of such a configuration and employs tiltable wings and rotors to combine take-off and landing flexibility with an efficient forward flight. This creates a highly complex take-off trajectory, where the dominant lift force gradually changes from propulsive thrust to the wing's circulation. An example of a tilt-wing configuration is Over-The-Wing Distributed Electric Propulsion (OTW-DEP). In this layout, the rotors are positioned over the suction side, with the rotor axes aligned with the wing's chord, see Figure 1.

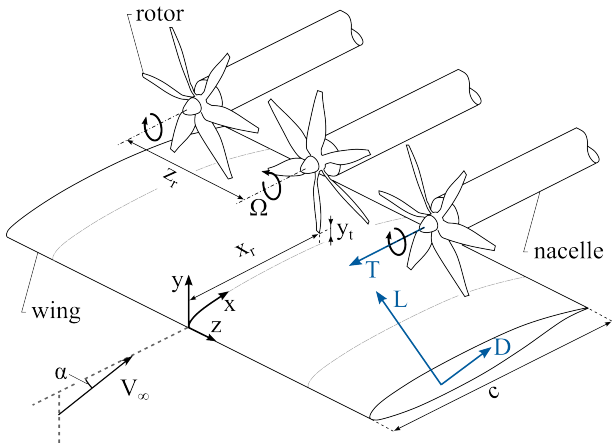

Figure 1: Schematic representation of over-the-wing propulsion with relevant system parameters and definition of aeropropulsive forces

A benefit of this rotor orientation is that the wing shields the rotor, effectively reducing fly-over noise [2]. Moreover, the rotors also induce a flow over the wing's suction side, leading to favorable aerodynamic charac-

teristics in the form of a lift increase [9] [5] and drag reduction [10]. A recent study [4] showed that such aero propulsive benefits on the component level translate to an increase in efficiency on the aircraft level by 9% .

The aerodynamic installation effects of tilt-wing systems, such as the OTW-DEP, are typically investigated by numerical simulation techniques and experimental measurements in wind tunnel facilities. Such aerodynamic interactions are typically expected to be quasi-steady. Therefore, the experiments are conducted for a fixed angle-of-attack and wind-tunnel velocity during acquisition [5] [8]. Furthermore, the flow physics during these experiments is revealed using velocimetry. Such techniques are usually limited to planar measurements, while the flow field around the rotors is three-dimensional and highly unsteady.

The current goal is to investigate the three-dimensional aerodynamic interactions of the OTW-DEP configuration during the transition from vertical to horizontal flight, and to identify the presence of any transient effects. For this, a time series of the flight conditions during the transition from vertical to horizontal flight is found using a reference eVTOL tilt-wing trajectory and integral loading measurements. This information is then used to conduct experiments in which the angle of attack and wind tunnel velocity vary dynamically. The aerodynamic interactions during this trajectory are then studied using time-resolved Lagrangian Particle Tracking and compared to measurements that are obtained for quasi-steady conditions.

2 Experimental arrangement

2.1 Windtunnel and model

The measurements are conducted in the Open-Jet Facility (OJF) at the High-Speed Laboratory at Delft University of Technology. The wind tunnel has an octagonal outlet of 2.85m width and 2.85m height. At the center of the outlet, a rotor-wing system is mounted vertically on a Quanser hexapod, see Figure 2. The wing model is a DLR-F15 high-lift device in retracted form, with a span of S = 0.95 m and chord of c = 0.24 m. The rotor array is positioned over the suction side of the wing at 60% chord and consists of five span-wise distributed, counter-rotating rotors with diameters of D = 0.127 m. The rotors' axes are parallel to the wing's chord line. The rotor's separation is $Z_r = 1.025D$ and the distance between the rotor tip and the wing's surface is $y_t = 0.135D$.

2.2 Lagrangian Particle Tracking

Volumetric velocity measurements cover the spatial domain as illustrated in Figure 2. The flow is seeded with HFSBs [6] that are illuminated by two LaVision LED Flashlight 300 devices at a distance of 0.6 m from the center of the measurement volume. A tomographic imaging setup is placed at 1.3 m from the model and consists of five high-speed (CMOS) cameras (PhotronFastcam SA1.1), equipped with lenses of focal lengths f = 60mm and set at numerical aperture of $f_\#$ = 12. System synchronization is obtained with a LaVision Programmable Timing Unit (PTU 8), and each measurement comprises 5457 recordings for a duration of 1.33 s. An overview of the measurement parameters is presented in Table 1.

Seeding type	HFSB
Camera type	5× Photron Fastcam SA1.1
Illumination	2× LaVision LED-Flashlight 300
Field of view (Δx, Δy,Δz)	50×50×25 cm^2
Repetition rate (Hz)	4000
Objective Focal length f (mm)	60
Numerical Aperture $f_\#$	12
Optical magnification M	0.05
Vector pitch (mm)	6

Table 1: Imaging and recording parameters eVTOL take-off study

The 3D particle motion analysis is performed with the Shake-The-Box method [11] and delivers approximately 18,000 particle tracks per time step. Data reduction to a Cartesian grid is obtained for each time step, by a sliding average in time over 99 snapshots ($t \approx 0.025$ s) during which the tracks are gathered in cubic bins of 24 mm size with a 75% overlap factor. Each bin comprises between 100 and 5000 samples and the resulting velocity field yields a spacing of 5 mm between neighboring vectors.

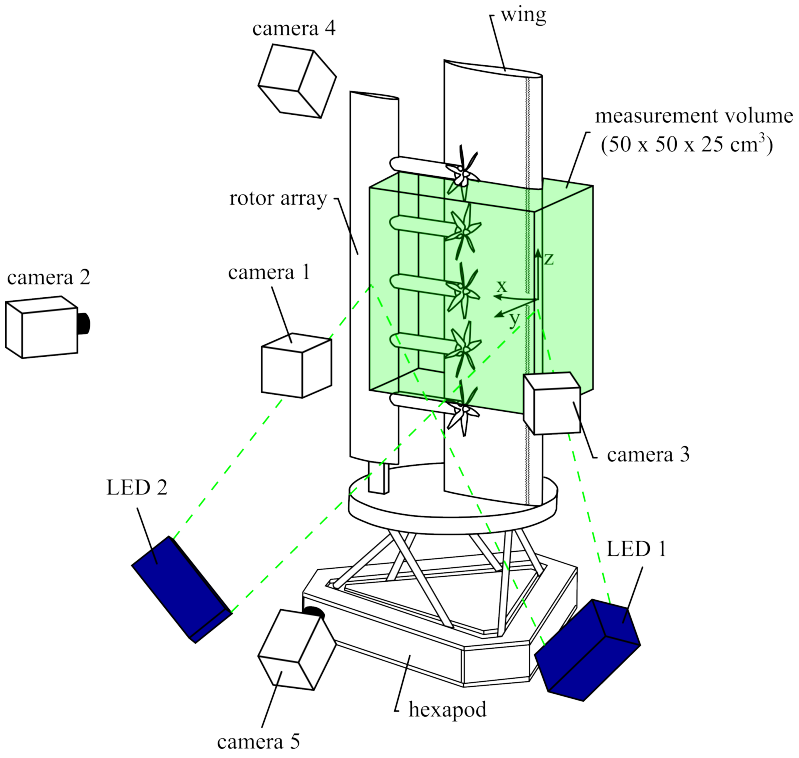

Figure 2: 3-D schematic of the experimental apparatus, coordinate system and measurement volume.

2.3 Operating conditions

To define the operating conditions, a reference tilt-wing flight envelope is chosen from literature [3] and scaled according to the wing span, see Figure 3 (left).

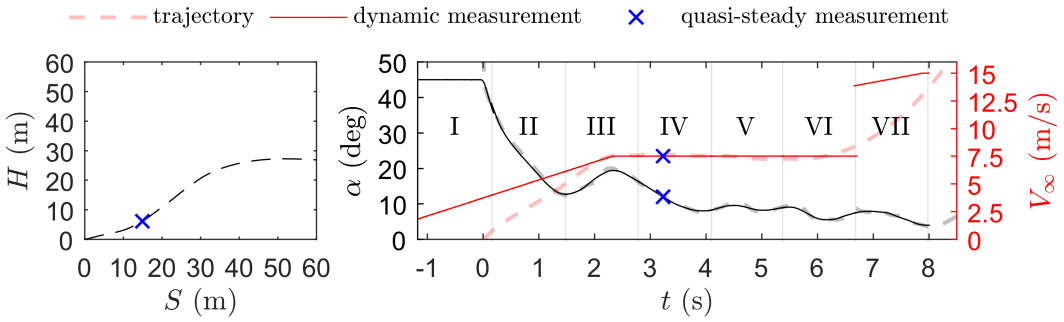

Figure 3: Left: Reference trajectory of eVTOL flight envelope. Right: Time series of the angle of attack and free-stream velocity and the discretization of the measurements.

Time series of the angle of attack α and free-stream velocity V_∞ that correspond to the current rotor-wing system are then found by using loading measurements which have been obtained [x] for a wide range of angles of attack and rotor advance ratios. Along the trajectory, a fixed rotation velocity of the rotors of Ω = 383 Hz is assumed. Hence the rotor advance ratio J is directly related to the free-stream velocity V_∞, i.e. $J = V_\infty/(\Omega D)$. To obtain the flight conditions that correspond to the reference flight trajectory, the time is discretized in steps of Δt = 0.005 s. For each time step t_i, a vertical and horizontal force balance is created by using the experimental rotors' thrust $T(V_\infty, \alpha)$ and wing lift $L(V_\infty, \alpha)$ and drag $D(V, \alpha)$. In this force balance, the vehicle mass m (corresponding to a maximum thrust-to-weight ratio of 0.8) and the angle of the rotor-wing system $\theta(t_i)$ with respect to the ground are also included:

$$F_x\left(t_i\right) = \sin\Big(\theta\left(t_i\right)\Big) \cdot T\Big(V_\infty\left(t_i\right), \alpha\left(t_i\right)\Big) - \sin\Big(\theta\left(t_i\right)\Big) \cdot F_{w,N}\Big(V_\infty\left(t_i\right), \alpha\left(t_i\right)\Big) + \cos\Big(\theta\left(t_i\right)\Big) \cdot F_{w,A}\Big(V_\infty\left(t_i\right), \alpha\left(t_i\right)\Big) - mg \quad (1)$$

$$F_y(t_i) = \cos\Big(\theta\left(t_i\right)\Big) \cdot T\Big(V_\infty\left(t_i\right), \alpha\left(t_i\right)\Big) - \cos\Big(\theta\left(t_i\right)\Big) \cdot F_{w,N}\Big(V_\infty\left(t_i\right), \alpha\left(t_i\right)\Big) - \sin\Big(\theta\left(t_i\right)\Big) \cdot F_{w,A}\Big(V_\infty\left(t_i\right), \alpha\left(t_i\right)\Big) \quad (2)$$

See Figure 4 for a schematic of the definition of the forces. Note that the wing's normal $f_{w,N}$ and axial force $f_{w,A}$ depend on the lift L and drag D of the wing only:

$$F_{w,N}\left(V,_\infty \alpha\right) = \sin\left(\alpha\right) \cdot L\left(V_\infty, \alpha\right) + \cos\left(\alpha\right) \cdot D\left(V_\infty, \alpha\right) \quad (3)$$

$$F_{w,A}\left(V_\infty, \alpha\right) = \cos\left(\alpha\right) \cdot L\left(V, \alpha\right) - \sin\left(\alpha\right) \cdot D\left(V, \alpha\right) \quad (4)$$

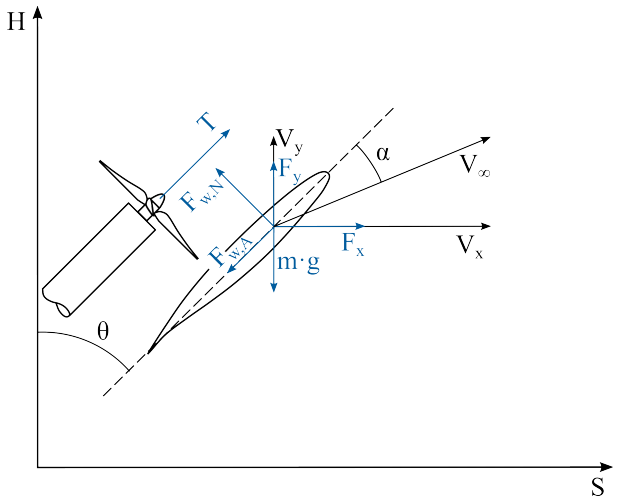

Figure 4: Definition of the force- (blue) and velocity-vectors (black) of the Over-The-Wing rotor system.

From equations 1 and 2, the horizontal and vertical velocities (V_x and V_y) and displacements (ΔS and ΔH) can be found. Corresponding to these velocities, the free-stream velocity $V_\infty(t_{i+1})$ and angle of attack $\alpha(t_{i+1})$ are updated, in which correction for unsteady effects is included through the Wagner function [x]. Finally, the angle of the rotor-wing system $\theta(t_{i+1})$ is updated in such a way that the vehicle follows the reference flight trajectory of Figure 3 (left). The found time series of the angle of attack α and velocity V_∞ are presented as the dotted lines in Figure 3 (right).

The measurements are then split into seven sequential measurements over the time series of the flight trajectory, see Figure 3 (right). The solid lines in the same figure present the measured angle of attack and wind tunnel velocity. Note that there are some discrepancies between the trajectory and measured values of the velocity V_∞. This is a result of the limited acceleration of the wind tunnel. Along the trajectory, a quasi-steady measurement is also performed for a fixed angle of attack and velocity of $\alpha = 12°$ and V_∞ = 7.5 m/s. The position of this measurement along the trajectory is indicated by the blue cross in Figure 3 (right).

3 Results

The flow physics of the rotor-wing system are presented in Figure 5 by the normalized velocity magnitude contours and velocity vectors in a vertical plane and over the surface of the wing. The vertical plane of the quasi-steady

results shows the induced velocity of the rotor and the contraction of the stream tube. The horizontal velocity contour plot shows that the flow is attached over the first half chord of the wing but is separated downstream by the adverse pressure gradient induced by the rotors.

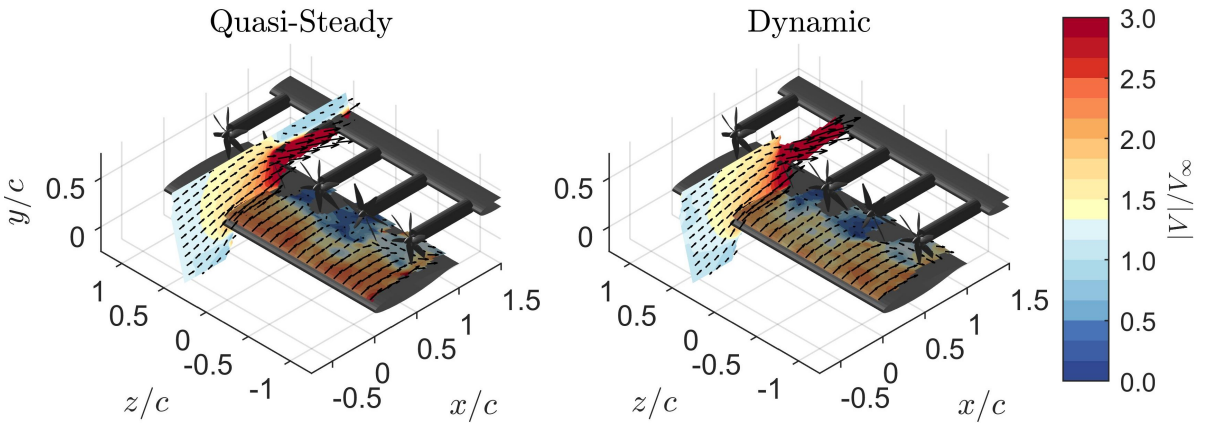

Figure 5: Normalized velocity magnitude $|V|/V_\infty$ and 2D velocity velocity vectors in the (x,y)-plane at $z/c = 0.45$ and over the wing's suction side extracted at $\Delta y = 0.08c$. The left side shows the quasi-steady results, while the right plot is generated for the dynamic operating conditions, both for $\alpha = 12$ and $V_\infty = 7.5$ m/s / $J = 0.15$.

The results of the dynamic measurements, presented on the right side in Figure 5, are extracted for the same operating condition as the quasi-steady results and present a similar flow topology. Nonetheless, the flow velocities near the wing's suction side are approximately 10% lower in magnitude.

4 Conclusions & Future work

An experimental campaign is conducted to study the three-dimensional aerodynamics of an over-the-wing mounted rotor system during an unsteady maneuver take-off maneuver. The operating conditions during a reference take-off trajectory have been found by using experimental loading measurements. The measurements return the three-dimensional aerodynamic interactions that occur during this dynamic variation of operating conditions. The rotors accelerate the flow over the wing but flow stagnation occurs at the chordwise position of the rotor. A velocity field snapshot which has been obtained under dynamically varying conditions and one where a fixed angle of attack has been described, show a similar flow topology. Velocities near the wing's surface are higher for the quasi-steady results but a more detailed analysis is required to conclude on the presence of any transient aerodynamic effects.

References

[1] Nicholas K Borer, Michael D Patterson, Jeffrey K Viken, Mark D Moore, JoeBen Bevirt, Alex M Stoll, and Andrew R Gibson. Design and performance of the nasa sceptor distributed electric propulsion flight demonstrator. In *16th AIAA Aviation Technology, Integration, and Operations Conference*, page 3920, 2016.

[2] EG Broadbent. Noise shielding for aircraft. *Progress in Aerospace Sciences*, 17:231–268, 1976.

[3] Shamsheer S Chauhan and Joaquim RRA Martins. Tilt-wing evtol takeoff trajectory optimization. *Journal of aircraft*, 57(1):93–112, 2020.

[4] Reynard de Vries and Roelof Vos. Aerodynamic performance benefits of over-the-wing distributed propulsion for hybrid-electric transport aircraft. *Journal of Aircraft*, 60(4):1201–1218, 2023.

[5] Hasse Dekker, Marthijn Tuinstra, Woutijn J Baars, Fulvio Scarano, and Daniele Ragni. Aeropropulsive performance modelling of over-the-wing propulsion at incidence. In *AIAA AVIATION 2023 Forum*, page 3355, 2023.

[6] David Engler Faleiros, Marthijn Tuinstra, Andrea Sciacchitano, and Fulvio Scarano. Generation and control of helium-filled soap bubbles for piv. *Experiments in Fluids*, 60:1–17, 2019.

[7] Rohit Goyal, Colleen Reiche, Chris Fernando, Jacquie Serrao, Shawn Kimmel, Adam Cohen, and Susan Shaheen. Urban air mobility (uam) market study. Technical report, 2018.

[8] Timothy Lee, T Ni, and Ge Lin. Aerodynamics and flowfield of distributed electric propulsion tiltwing during transition with deflected trailing-edge flap. *Journal of Fluids Engineering*, 146(5), 2024.

[9] Emanuel A Marcus, Reynard de Vries, Akshay Raju Kulkarni, and Leo L Veldhuis. Aerodynamic investigation of an over-the-wing propeller for distributed propulsion. In *2018 AIAA Aerospace Sciences Meeting*, page 2053, 2018.

[10] Lars Müller, Wolfgang Heinze, Dragan Kožulović, Martin Hepperle, and Rolf Radespiel. Aerodynamic installation effects of an over-the-wing propeller on a high-lift configuration. *Journal of Aircraft*, 51(1):249–258, 2014.

[11] Daniel Schanz, Sebastian Gesemann, and Andreas Schröder. Shake-the-box: Lagrangian particle tracking at high particle image densities. *Experiments in fluids*, 57:1–27, 2016.